

Article

# Heterogeneous Synergistic Catalysis for Promoting Aza-Michael–Henry Tandem Reaction for the Synthesis of Chiral 3-Nitro-1,2-Dihydroquinoline

Zhe An, Lifeng Chen, Yitao Jiang and Jing He \* 

State Key Laboratory of Chemical Resource Engineering &amp; Beijing Advanced Innovation Center for Soft Matter Science and Engineering, Beijing University of Chemical Technology, Beijing 100029, China

\* Correspondence: hejing@mail.buct.edu.cn; Tel.: +861064425280

Received: 5 August 2019; Accepted: 21 August 2019; Published: 24 August 2019



**Abstract:** Heterogeneous synergistic catalysis by SBA-15 immobilized chiral amines catalysts has promoted efficient aza-Michael–Henry tandem reaction for the synthesis of chiral 3-Nitro-1,2-Dihydroquinoline. Final products in the asymmetric aza-Michael–Henry cascade reactions between 2-aminobenzaldehyde and  $\beta$ -nitrostyrene were afforded in a yield of 85% and an enantiomeric excess (ee) value of 98% on (S)-(-)-2-aminomethyl-1-ethylpyrrolidine immobilized SBA-15. SBA-15-AEP catalyst has been also extended to the asymmetric aza-Michael–Henry cascade reaction of substituted R1-2-aminobenzaldehyde and R2-substituted nitroolefin. The heterogeneous synergistic mechanism for both tertiary amine and secondary amine immobilized mesoporous has been proposed in detail including the geometrical constraints in the ee promotion.

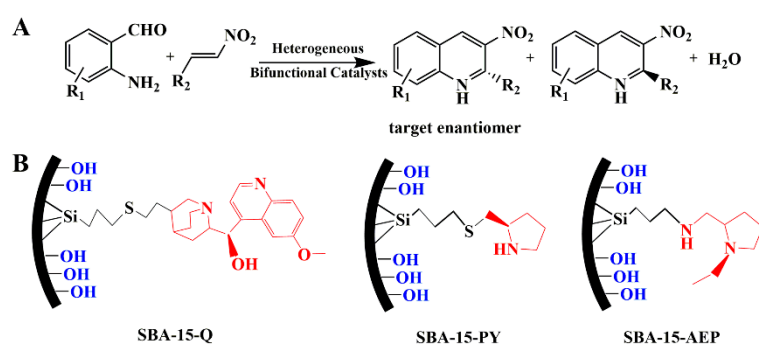
**Keywords:** heterogeneous asymmetric catalysis; bi-functional; 3-nitro-1,2-dihydroquinoline; tandem reaction; synergistic effects

## 1. Introduction

Dihydroquinoline compounds [1,2] are widely found in various natural products that possess diverse biological and pharmacological activities [3–5]. Especially for 1,2-Dihydroquinoline compounds, they gain more extensive attention since they are not only the intermediates for the synthesis of Skraup quinolones [6] in the field of pharmaceuticals but also they have significant applications in the fields of agrochemicals and chemicals [7,8]. For example, the global consumption of dihydroquinoline reached 100 thousand tons only as rubber antioxidant in 2010 and 10 thousand tons only as food-antioxidant in 2013 [9,10], respectively. However, a large proportion of bioactive hydroquinoline products [11,12], taking mefloquine and angusturine for example, are utilized in racemic form. In fact, hydroquinoline enantiomers are found to display distinctly different properties [13,14]. Therefore, it is important to produce optically pure hydroquinoline enantiomer. Current industrial methods, including the extraction from coal tar [15] and the classic chemical synthesis [16–18], are difficult to meet the asymmetric production requirements. The classic chemical synthesis methods, including Skraup Doebner–Von Miller, Combes, etc., usually use the inorganic acid as catalyst, such as sulfuric acid or concentrated hydrochloric acid, which brings enormous environmental stress. Therefore, the development of effective and environment-friendly methods to synthesize the enantioselective hydroquinoline compounds is of considerable ongoing interest and currently highly desired [6,19,20].

The asymmetric catalytic synthesis of quinoline derivatives by using chiral organometallic compounds as catalysts has been intensively investigated [21–23]. Particularly, the asymmetric hydrogenation reactions employing Rh, Pd, and Ir complexes as catalysts have been demonstrated to be efficient enough to afford chiral quinoline derivatives [24–26]. Then the organocatalysts have

been focused on because of their high efficiency and metal-free nature [27]. Usually, single-site organocatalysts could perform well only by coordinating with co-catalysts or assistant catalysts [28]. Córdova et al. [29] employed diphenylprolinol trimethylsilyl ethers as catalysts with benzoic acid as cocatalyst to synthesize chiral 1,2-dihydroquinolines by the aza-Michael–Aldol reaction between 2-aminobenzaldehydes and  $\alpha$ ,  $\beta$ -unsaturated aldehydes. Soon afterwards, Wei [30] and Hamada et al. [31] promoted the selectivity of the aza-Michael–Aldol reaction through intensifying the nucleophilicity and the steric hindrance of the substrate by changing 2-aminobenzaldehydes to N-protected 2-aminobenzaldehydes. The reaction conversion was also reported to be increased with the assistance of sodium acetate or acetic acid. Later, Xu et al. [32] disclosed the first organocatalyzed enantioselective domino aza-Michael–Henry reaction employing bi-functional primary amine thiourea as catalyst and benzoic acid as cocatalyst, achieving a yield of 70% and an enantiomer excess (ee) value of 85% of 3-nitro-1,2-dihydroquinolines. Subsequently, Lu et al. [33] developed a quinidine-derived tertiary amine-thiourea catalyst catalyzing a similar aza-Michael–Henry reaction, affording a yield of 92% and an ee value of 90%. They modified an electron-withdrawing sulfone group on the amino moiety of 2-aminobenzaldehyde to increase the aniline N–H acidity and induce asymmetric reaction by the steric hindrance of the sulfonamide. Despite the great advances so far, the asymmetric synthesis of quinoline derivatives from the substrates without protected or modified N is still a great challenge, and in most cases an acidic additive or co-catalyst is required for achievement of impressive catalytic efficacy. Here, we propose a heterogeneous acid–base synergistic catalysis route on the asymmetric synthesis of quinoline derivatives by an aza-Michael–Henry cascade reaction (Scheme 1A), employing a heterogeneous bi-functional catalyst with inherent achiral silanols of mesoporous silica as acidic sites and immobilized chiral amines as basic sites (Scheme 1B). The final product is afforded in up to a yield of 85% and an ee value of 98%.



**Scheme 1.** (A) Asymmetric aza-Michael–Henry cascade reaction and (B) the designed heterogeneous bi-functional catalysts.

Heterogeneous acid–base bi-functional catalysts have been reported to promote asymmetric reactions successfully with good activity and high enantioselectivity [34], which could well solve the tough problem of mutual deactivation [35] of acid and base sites in homogeneous counterparts. Immobilized acid and base active sites could supply efficient synergistic catalysis as previously reported [36–41]. Our group more recently reported efficient synergistic catalysis achieved with inherent achiral silanols of mesoporous silica as acidic sites and immobilized chiral amines as basic sites in the direct asymmetric aldol condensation [42], the asymmetric Henry–Michael one-pot reaction [43], oxa-Michael–Michael cascade reaction [44] and Knoevenagel–phospha-Michael tandem reaction [45]. The heterogeneous bi-functional catalysts were not only demonstrated effective in the synergistic catalysis, but also were easy to be separated and recycled. Inspired by our previous reports, here the challenges in the synthesis of optically pure quinoline derivatives by asymmetric cascade reaction are to be dealt with by using the heterogeneous bi-functional catalysts.

Quinine and pyrrolidine have been attempted as homogeneous catalysts for the synthesis of chiral quinoline derivatives [24–27], while found to be inefficient unless accompanied or assisted with acidic

sites. So this work chooses quinine (tertiary amine, abbreviated as Q) and (S)-(+)-prolinol (secondary amine, abbreviated as PY) as the grafted amine. Then (S)-(-)-2-aminomethyl-1-ethylpyrrolidine (abbreviated as AEP), which bears both of tertiary and secondary amine sites, with a structure simpler than quinine while more complex than pyrrolidine, was grafted as the precursor of basic sites. The heterogeneous catalysts are respectively abbreviated as SBA-15-Q, SBA-15-PY, and SBA-15-AEP, as shown in Scheme 1B.

## 2. Results and Discussion

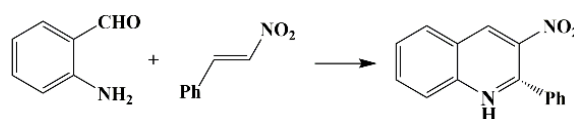
To anchor the selected amines, thiol/bromine functionalized materials, abbreviated as SBA-15-SH and SBA-15-Br, were first prepared by post-synthesis grafting reaction. SBA-15-SH or SBA-15-Br well preserves the well-ordered long-range structure of SBA-15 precursor, with (100), (110) and (200) reflections clearly observed in the powder X-ray diffraction (XRD) patterns (Figures S1 and S2). The N<sub>2</sub> adsorption–desorption isotherms typical of type IV with H1 hysteresis loop are observed for SBA-15-SH and SBA-15-Br (Figures S3 and S4). The pore size distribution of SBA-15-SH or SBA-15-Br remains as narrow as that of SBA-15 (Figures S3 and S4). Well-ordered mesoporous channels are clearly observed from TEM images (Figure S5) for SBA-15 as well as SBA-15-SH and SBA-15-Br, confirming the well-ordered mesoporous structures. The slight decrease in the specific surface area and pore volume (Table S1) indicates that the grafted functional groups are located inside the mesopores. The immobilization of chiral amines was achieved by the reactions between  $\text{C}=\text{C}/\text{OH}$  and  $\text{SH}$ , or between  $\text{NH}_2$  and  $\text{Br}$  following the methods reported in [46]. The <sup>13</sup>C CP/MAS nuclear magnetic resonance (NMR) spectra clearly indicate the successful immobilization of functional groups (Figures S6–S8). No signals of double bonds are observed at 114 ppm for SBA-15-Q, indicating the complete reaction of double bonds with the surface mercapto groups. The alkyl carbon signals of PY and AEP are observed at 20–60 ppm and 10–70 ppm. The chemical shift and relative intensity well match the structures of grafted moieties. The resulting SBA-15-Q, SBA-15-PY, and SBA-15-AEP possess well-ordered mesoporous structure according to the results of XRD patterns, N<sub>2</sub> adsorption–desorption experiments, and TEM images (Figures S1–S5). The amount of loaded N for SBA-15-Q, SBA-15-PY, and SBA-15-AEP is respectively calculated to be 0.829, 0.639, and 0.829 mmol/g from the elemental analysis (Table S2). According to the specific surface areas and the N atom number in the basic sites, the density of grafted amines is respectively calculated to be 1.074, 0.707, and 0.693 μmol/m<sup>2</sup> (Table S2). The silanol density of SBA-15-SH and SBA-15-Br was calculated to be 4.46 and 8.87 μmol/m<sup>2</sup> (Table S3) determined by the deconvolution of <sup>29</sup>Si MAS NMR signals (Figure S9) and the specific surface areas (Table S1). The molar ratio of surface silanols to immobilized amines for SBA-15-Q, SBA-15-PY, and SBA-15-AEP is respectively calculated to be 4:1, 6:1 and 13:1. The possible reason for the highest molar ratio of surface silanols to immobilized amines for SBA-15-AEP may be the largest steric hindrance near the surface caused by the ethyl-substituted ring after 5 C atoms.

SBA-15-Q, SBA-15-PY, and SBA-15-AEP were then applied in the asymmetric aza-Michael–Henry cascade reaction between 2-aminobenzaldehyde and β-nitrostyrolene (Table 1). Preliminary investigation in CH<sub>3</sub>OH solvent demonstrates the occurrence of asymmetric aza-Michael–Henry cascade reaction on SBA-15-Q, SBA-15-PY, and SBA-15-AEP, affording 86%, 60%, and 83% ee values (Table 1, entries 1–3). The yield on SBA-15-PY is higher than on SBA-15-Q, while ee value is on the contrary. For SBA-15-AEP, with both secondary and tertiary amine sites, the yield is higher than on either individual secondary or tertiary amine, while the ee value is similar to that on SBA-15-Q. Increasing reaction temperature causes a slight loss of ee value while promoting the yield visibly (Table 1, entry 4). The yield at 40 °C approaches a similar value in 24 h to that in 48 h at 35 °C (40% versus 49%). Both yield and enantioselectivity increase by using *i*-PrOH as solvent (Table 1, entries 5 and 6), which was similar to the homogeneous system reported by Xu et al. [47]. The yield further rises by extending the reaction time without visible loss of ee value (Table 1, entry 7).

In *i*-PrOH solvent, SBA-15-Q, possessing tertiary amine center, affords a yield of 37% in 72 h at 40 °C with an ee value of 99% (Table 2, entry 1), with the ee value much higher than the homogeneous

counterpart (Table 2, entry 2) under the same reaction condition. The yield afforded by SBA-15-Q is lower than the homogeneous counterpart (Table 2, entries 1 and 2), but higher than that observed on the heterogeneous catalyst passivated by post-silylation (SBA-15-Q-CH<sub>3</sub>) (Table 2, entry 3). The sharp decrease in the yield resulting from the post-silylation clearly indicates the crucial role of surface silanols in the enhancement of catalytic activity, just as expected in the synergistic catalysis strategy. The post-silylation also causes a decrease in the ee value (from 99% to 70%), indicating that the participation of surface silanols in the catalysis promotes the enantioselectivity as well in spite of the achiral acid species. Similar results are observed for SBA-15-PY and SBA-15-AEP. SBA-15-PY affords higher ee value (Table 2, entry 4) than both of homogeneous counterpart (Table 2, entry 5) and SBA-15-PY-CH<sub>3</sub> (Table 2, entry 6). SBA-15-AEP (Table 2, entry 7) affords an ee value of 98%, while the homogeneous counterpart affords an ee value of only 8% (Table 2, entry 8). The immobilization of AEP on the SBA-15 significantly remarkably promotes the enantioselectivity. SBA-15-AEP-CH<sub>3</sub> affords an ee of 40% (Table 2, entry 9), which is visibly lower than that on SBA-15-AEP though higher than that achieved on the homogeneous counterpart. Both SBA-15-PY (Table 2, entry 4) and SBA-15-AEP (Table 2, entry 7) afford visibly higher yield than their respective passivated counterparts SBA-15-PY-CH<sub>3</sub> (Table 2, entry 6) and SBA-15-AEP-CH<sub>3</sub> (Table 2, entry 9), further indicating the promotion of silanol cooperation to the catalytic activity. SBA-15-SH (Table 2, entry 10) or SBA-15-Br (Table 2, entry 11), as the precursor to anchor the basic moieties, could scarcely establish the reaction, revealing the single acid site could not catalyze the reaction without base in comparison with the result of no catalyst added (Table 2, entry 12). Therefore, the expected synergistic catalysis between the achiral surface silanols of mesoporous support and chiral amines has been demonstrated on the heterogeneous catalysts in this work.

**Table 1.** The aza-Michael–Henry cascade reaction on designed bi-functional catalysts with tailored reaction conditions.



Entry	Catalyst	T (°C)	Solvent	Time (h)	Yield (%) <sup>a</sup>	EE (%) <sup>b</sup>
1	SBA-15-Q	35	CH <sub>3</sub> OH	48	19	86
2	SBA-15-PY	35	CH <sub>3</sub> OH	48	36	60
3	SBA-15-AEP	35	CH <sub>3</sub> OH	48	49	83
4	SBA-15-AEP	40	CH <sub>3</sub> OH	48	54	75
6	SBA-15-AEP	40	<i>i</i> -PrOH	48	70	99
7	SBA-15-AEP	40	<i>i</i> -PrOH	72	85	98

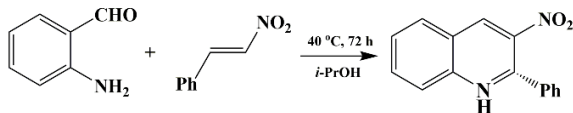
Unless indicated otherwise, all the reactions were performed with 0.1 mmol of 2-aminobenzaldehyde, 0.12 mmol of  $\beta$ -nitrostyrene, and cat. (20 mol %) in 1 mL of solvent. <sup>a</sup> Determined by <sup>1</sup>H NMR. <sup>b</sup> Determined by high performance liquid chromatography (HPLC).

The heterogeneous catalysts all presents a decrease yield in the same reaction time compared with the corresponding homogeneous counterparts probably due to the diffusing resistance of the SBA-15 mesopores. However, SBA-15-AEP with the largest dimensional size of immobilized amine among the three catalysts establishes the highest yield in the heterogeneous catalysis. It is proposed that the yield for the heterogeneous catalyst also depends on the surface silanol/immobilized amine. For SBA-15-AEP with the highest surface silanol/amine (13:1) achieves a lowest decrease from the homogeneous counterparts among the three catalysts. From the viewpoint of the enantioselectivity, SBA-15-Q (from 10% of Q to 99%) and SBA-15-AEP (from 8% of AEP to 98%) catalysts possessing tertiary amine structure promote the asymmetric cascade reaction more efficiently than SBA-15-PY with individual secondary amine (from 15% of PY to 71%). We propose that the pore walls of SBA-15 impose steric effects, similar to what has been found by Jones and co-workers in the heterogeneous Rh(I)-catalyzed asymmetric hydrogenation [48]. SBA-15-P123-AEP (Table 2, entry 13), in which the template P123 was not removed from the internal mesopores and the (S)-(-)-2-aminomethyl-1-ethylpyrrolidine was

grafted on the outside surface of the SBA-15, was then prepared to further confirm the steric effects within the confined space. An ee value of 25% was obtained that is lower than SBA-15-AEP (98%) but higher than the homogeneous (S)-(-)-2-aminomethyl-1-ethylpyrrolidine (8%) (Table 2, entry 13). More interesting is that the enantioselectivity promotion with the participation of surface silanols for SBA-15-AEP (from 40% of SBA-15-AEP-CH<sub>3</sub> to 98%) is the greatest among the three catalyst. The synergistic catalysis promotes the heterogeneous reaction more efficiently with more silanol groups around the amine sites.

The heterogeneous bi-functional catalyst SBA-15-AEP designed in this work could be extended to the asymmetric aza-Michael–Henry cascade reaction of substituted R<sub>1</sub>-2-aminobenzaldehyde and R<sub>2</sub>-substituted nitroolefin (Table 3). The substituted R<sub>2</sub>-substituted nitroolefin (entries 1–4) and R<sub>1</sub>-2-aminobenzaldehyde (entries 5–7) were found to be tolerated in this cascade reaction. It reveals that the substrates with electron-withdrawing substituents are more favored than that with electron-donating substituents of 2-aminobenzaldehyde in the heterogeneous aza-Michael–Henry cascade reactions.

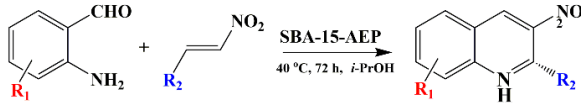
**Table 2.** The aza-Michael–Henry cascade reaction on designed bi-functional catalysts in *i*-PrOH at 40 °C for 72 h.



Entry	Catalyst	Yield (%) <sup>a</sup>	EE (%) <sup>b</sup>
1	SBA-15-Q	35 (39)	99 (99)
2	Q	50	10
3	SBA-15-Q-CH <sub>3</sub>	10	70
4	SBA-15-PY	40 (41)	71 (72)
5	PY	>99	15
6	SBA-15-PY-CH <sub>3</sub>	20	65
7	SBA-15-AEP	85 (81)	98 (98)
8	AEP	>99	8
9	SBA-15-AEP-CH <sub>3</sub>	42 (45)	40 (42)
10	SBA-15-SH	3	14
11	SBA-15-Br	3	16
12	-	2	13
13	SBA-15-P123-AEP	39	25

<sup>a</sup> Determined by <sup>1</sup>H NMR. <sup>b</sup> Determined by HPLC. The data in parentheses are reproduced results.

**Table 3.** Substrate scope for SBA-15-AEP catalyzed aza-Michael–Henry cascade reactions.



Entry	R <sub>1</sub> Group	R <sub>2</sub> Group	Yield (%) <sup>a</sup>	EE (%) <sup>b</sup>
1	H	2,3-MeO-Ph	67 (65)	98 (98)
2	H	4-Me-Ph	60 (59)	90 (93)
3	H	2,4-Cl-Ph	45 (40)	97 (96)
4	H	3,4-Cl-Ph	42 (38)	95 (97)
5	3-MeO	Ph	52 (50)	95 (99)
6	5-Cl	Ph	55 (53)	98 (99)
7	3,5-Br	Ph	68 (67)	99 (98)

<sup>a</sup> Determined by <sup>1</sup>H NMR. <sup>b</sup> Determined by HPLC. The data in parentheses are reproduced results.

Catalyst recycling has also been explored. The heterogeneous catalyst could be recovered by simple centrifugation. The catalytic property catalyzed by SBA-15-AEP in the aza-Michael–Henry cascade reactions between 2-aminobenzaldehyde and β-nitrostyrolene stayed at the same level after five runs

(Figure 1). The content of N for reused SBA-15-AEP in five runs was measured to be 0.620 mmol/g and almost no leaching was observed. Figure S10 indicates the recovered catalysts still possess the long-range and periodic ordered mesoporous structures. The N<sub>2</sub> adsorption–desorption isotherms typical of type IV with H1 hysteresis loop and well-distributed pore size distribution are still observed for used SBA-15-AEP (Figure S11). The scaling experiments with 10 times (1.0 mmol of 2-aminobenzaldehyde and 1.2 mmol of  $\beta$ -nitrostyrene) and 100 times (10.0 mmol of 2-aminobenzaldehyde and 12.0 mmol of  $\beta$ -nitrostyrene) have been carried out in order to further illustrate the synthetic value of this methodology. The catalyst achieved a yield of 94% and an ee value of 97% at the same level with 1.0 mmol of 2-aminobenzaldehyde.

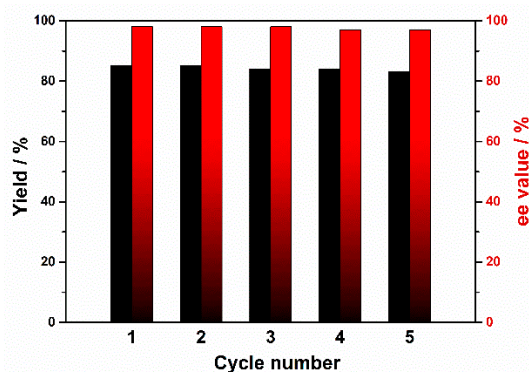


**Figure 1.** The recycling of the SBA-15-AEP catalyst in the aza-Michael–Henry cascade reaction between 2-aminobenzaldehyde and  $\beta$ -nitrostyrene.

The heterogeneous catalysts achieve high enantioselectivity in the aza-Michael–Henry cascade reaction, presumably resulting from the geometrical constraints of mesoporous support that accompany the formation of the intermediate. It is found that SBA-15-Q and SBA-15-AEP possessing tertiary amine structure promote the asymmetric cascade reaction more efficiently than SBA-15-PY with individual secondary amine. Based on the above analysis and the previous reports [49–51], the heterogeneous mechanism for SBA-15 immobilized secondary amine (Figure 2) and tertiary amine (Figure 3) has been proposed respectively. For SBA-15-PY (Figure 2), firstly in the aza-Michael reaction, secondary amine reacts as a nucleophile with the carbonyl group of 2-aminobenzaldehyde to form iminium ions giving H<sub>2</sub>O [52].  $\beta$ -nitrostyrene is activated by the surface silanols as hydrogen-bonding donor, which is helpful to connect the electrophile to the iminium-activated 2-aminobenzaldehyde in the transition state [49]. Then the N of amino group in the iminium intermediate nucleophilically attacks the  $\alpha$ -C in the activated  $\beta$ -nitrostyrene and abstracts H from amino-group to form the stereoselectivity. The steric hindrance of mesopore wall remarkably constrains the *Re*-face activation of  $\beta$ -nitrostyrene close to the mesopore wall, leaving the *Si*-face attacking pathway in green. As a result, improved ee value could be achieved compared with the homogeneous process. Then in the subsequent intramolecular Henry reaction, the  $\beta$ -C in the activated  $\beta$ -nitrostyrene nucleophilically attacks the tautomeric enamine with the hydration of the N–H bonding followed by intramolecular dehydration to form the final product and recover the heterogeneous catalyst.

For SBA-15 immobilized tertiary amine (Figure 3), firstly in the aza-Michael reaction, the tertiary amine interacts with aniline N–H to form hydrogen bond to activate the amino group [49].  $\beta$ -nitrostyrene is also activated by the surface silanols as hydrogen-bonding donor. Then the amino group nucleophilically attacks the  $\alpha$ -C in the activated  $\beta$ -nitrostyrene and abstracts H from amino-group, forming the stereoselectivity. Similar to the secondary amine catalyzed mechanism, the steric hindrance constrains the *Re*-face attacking pathway that close to the mesopore wall, leaving the *Si*-face attacking pathway in green. However, compared with secondary amine, the activation mode by the tertiary amine makes the amino group possessing fewer degrees of freedom, which is better for the establishment of stereoselectivity. As a result, a more remarkable ee value enhancement could

be achieved for SBA-15-Q and SBA-15-AEP than SBA-15-PY. Then in the subsequent intramolecular Henry reaction, the  $\beta$ -C in the activated  $\beta$ -nitrostyrene nucleophilically attacks the C of carbonyl group followed by intramolecular dehydration to form the final product and recover the heterogeneous catalyst. In addition, because SBA-15-AEP is of the most surface silanol, the activation capacity for  $\beta$ -nitrostyrene is deduced to be strongest, thus resulting in the greatest product yield.

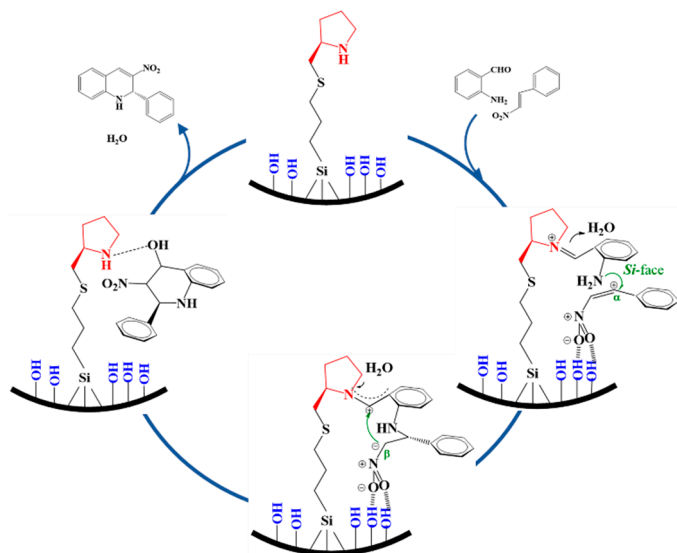


**Figure 2.** The proposed heterogeneous catalytic mechanism for SBA-15-PY in the aza-Michael–Henry cascade reaction.

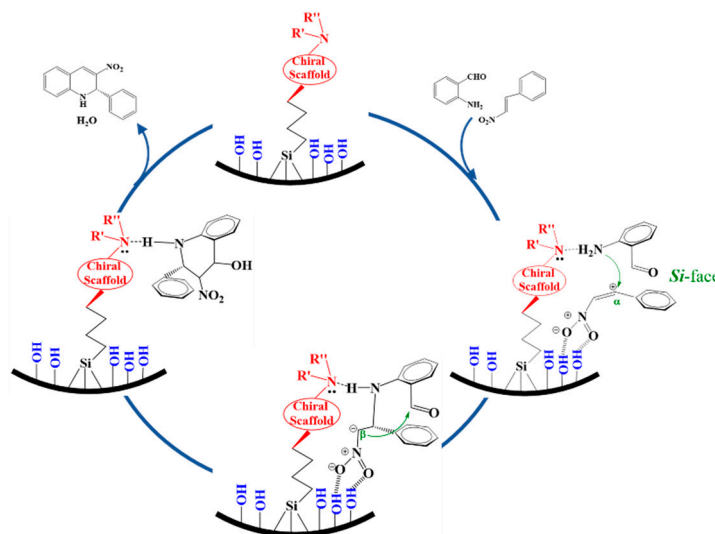


**Figure 3.** The proposed heterogeneous catalytic mechanism for SBA-15 immobilizing tertiary amine in the aza-Michael–Henry cascade reaction.

### 3. Experimental

#### 3.1. Materials and Characterizations

P123 ( $\text{EO}_{20}\text{PO}_{70}\text{EO}_{20}$ , molecular weight 5800), (S)-(+)-prolinol, Diphenylphosphine, prolinol, 3-merrapnpropyltrimethnxysilane (MPTMS), Tetraethyl orthosilicate (TEOS), (3-bromopropyl) trichloro-Silane, Quinine, and  $\beta$ -nitrostyrene were purchased from Sigma-Aldrich (Burlington, MA, USA) or Alfa-Aesar (Shanghai, China). 2-Aminobenzaldehyde, 2-amino-3-methoxy-Benzaldehyde, 2-amino-5-chloro-Benzaldehyde, 2,4-dichloro- $\beta$ -nitrostyrene, 3,4-dichloro- $\beta$ -nitrostyrene, 2,3-dimethoxy-

$\beta$ -nitrostyrene and (S)-(-)-2-Aminomethyl-1-ethylpyrrolidine were purchased from J&K Chemical company with 98% purity (Shanghai, China). All the reagents and commercial chemicals were used as received.

XRD patterns were carried out on a D8 focus X-ray diffractometer (Bruker, Berlin, German) with Cu  $K_{\alpha}$  radiation (30 mA, 45 kV). Nitrogen adsorption/desorption experiments were obtained on an Autosorb-1 system (Quantachrome, Chicago, IL, USA). Before measurements, the samples were outgassed at 80 °C for 8 h. The specific surface areas were calculated using the Brunauer–Emmett–Teller (BET) method and the mesopore size distribution was calculated using the Barret–Joyner–Halenda (BJH) method from the desorption branches of nitrogen isotherms. Transmission electron microscopy (TEM) images were recorded on 2100 high-resolution transmission electron microscopes (JEOL, Tokyo, Japan). Before measurements, samples were dispersed in ethanol and subsequently deposited on a microgrid. Elemental analysis of C, H, N, and S was performed using a VarioEL (Elementar Analysensysteme GmbH, Langensfeld, German) elemental analyzer.  $^1\text{H}$  and  $^{13}\text{C}$  NMR spectra were obtained on an Avance 400 MHz NMR spectrometer (Bruker, Berlin, Germany). The solid-state NMR experiments were carried out on an Avance 300 MHz solid-state spectrometer (Bruker, Berlin, Germany) with a commercial 4 mm MAS NMR probe at frequencies of 75.5 and 59.6 MHz for  $^{13}\text{C}$  CP/MAS.  $^{29}\text{Si}$  BD-MAS NMR spectra for the silanol determination were carried out using an Hpddec pulse sequence, which is one pulse sequence with a high-power proton decoupling. Silanol concentrations were calculated by dividing the molar fraction of the  $\text{Q}^i$  ( $\text{Q}^i = \text{Si}(\text{OSi})_i(\text{OH})_{4-i}$ ,  $i = 2-4$ ,  $-80$  to  $-130$  ppm) species by the molar weight of the sample (determined as sum of molar weights and fractions of the  $\text{Q}^i$ ). Before measurements, the samples were vacuumed to remove water and exclude the surface hydration. HPLC analysis was performed on Prostar 210 HPLC (Varian, Palo Alto, CA, USA) with Prostar 325 UV–Vis detector.

### 3.2. Catalysts Preparation

**Preparation of SBA-15:** Mesoporous silica, SBA-15, was synthesized following the procedure following the procedure reported by Zhao et al. [46]. Firstly, 4.0 g of the temple P123 was dissolved in a 128 mL of HCl and deionized  $\text{H}_2\text{O}$  mixture under stirring at 40 °C. Then, 8.54 g of TEOS was slowly added into the solution when P123 completely dissolved, followed by slow stirring for 20 h at 45 °C. The resulting mixture was maintained at 100 °C under static condition for 48 h, and then filtered and dried. Template removing was conducted under calcination at 550 °C for 6 h.

**SBA-15-SH [52–54]:** Dried SBA-15 (0.8 g) and (3-mercaptopropyl) trimethoxysilane (1.2 mL) were added to anhydrous toluene (24 mL) and heated at 110 °C for 24 h. Then the solid was filtered, thoroughly washed, and dried in vacuo for 12 h.

**SBA-15-Br [48]:** Dried SBA-15 after vacuum treatment (1.0 g) was suspended in 7.5 mL of anhydrous tetrahydrofuran (THF). Then, 3-Bromopropyltrichlorosilane (2.4 mmol) was added into the cooled slurry at  $-78$  °C. The mixture was slowly warmed up, and then stirred at 25 °C for 8 h and at 50 °C for another 1 h. Then the solid was filtered, treated by the Soxhlet extraction using THF, and dried in vacuo for 12 h.

**SBA-15-Q [45]:** Dried SBA-15-SH (1.0 g), quinine (0.5 g) and  $\alpha, \alpha'$ -azoisobutyronitrile (AIBN, 50 mg) in 25 mL of chloroform was refluxed under  $\text{N}_2$  atmosphere for 24 h. The solid was filtered, thoroughly washed and dried in vacuo.

**SBA-15-Py [45]:** Dried SBA-15-SH (1.0 g), 4-methyl benzenesulfonic acid (52.1 mg) and (S)-(+)-prolinol (83.1 mg) in 30 mL of anhydrous toluene was refluxed under  $\text{N}_2$  atmosphere for 48 h. The solid was filtered, thoroughly washed and dried in vacuo.

**SBA-15-AEP [45]:** Dried SBA-15-SH (1.0 g) and (S)-(-)-2-aminomethyl-1-ethylpyrrolidine (150mg) in 15 mL of anhydrous toluene was stirred at 50 °C for 48 h. The solid was filtered, treated by Soxhlet extraction using THF, and dried in vacuo.

**SBA-15-Base-CH<sub>3</sub> (Base = PY, AEP, Q):** Dried SBA-15-SH (1.0 g) and trimethylmethoxysilane (2 mL) in 50 mL of anhydrous toluene (50 mL) was refluxed under N<sub>2</sub> atmosphere for 24 h. The solid was filtered, thoroughly washed and dried in vacuo.

**SBA-15-P123-AEP:** SBA-15 without removing the template P123 from the internal mesopores was used as the precursor for SBA-15-P123-AEP. The calcination procedure at 550 °C for 6 h for as prepared SBA-15 was not needed. The preparation procedure was the same as for SBA-15-AEP mentioned above.

### 3.3. Aza-Michael–Henry Cascade Reaction

Firstly, 0.10 mmol of 2-aminobenzaldehyde, 0.12 mmol of  $\beta$ -nitrostyrolene, and 20 mol% of catalyst were mixed in 1 mL of solvent. Then the mixture was heated to 40 °C and stirred for 72 h if not specially indicated. The reaction product was isolated by chromatographic purification. The yield was determined by <sup>1</sup>H NMR analysis with 0.1 mmol of 1,1,2,2-tetrachloroethane (6.00 ppm) as the internal standard. Through calculating the ratio for integral area of the target product with 1,1,2,2-tetrachloroethane, the yield of the target product was obtained according the previous report [55]. The ee values were measured by HPLC with Chiralpak OD-H column using isopropanol/n-hexane (v/v = 15/85) as flow phase at a flow rate of 1.0 mL/min in the detection wavelength of 254 nm.

## 4. Conclusions

In conclusion, we have developed the heterogeneous acid–base bi-functional catalyst for the enantioselective aza-Michael–Henry cascade reaction of nitroolefins and 2-aminobenzaldehydes. The synergistic catalysis between inherent achiral silanols of mesoporous silica as acidic sites and immobilized chiral amines as basic sites allows this challenging transformation to take place under mild reaction conditions. The final product is afforded in up to 85% yield and 98% ee. The effects of substituents of 2-aminobenzaldehyde and nitroolefin have been also investigated. The heterogeneous synergistic mechanism for both tertiary amine and secondary amine immobilized mesoporous has been proposed in detail including the geometrical constraints in the ee promotion.

**Supplementary Materials:** The following are available online at <http://www.mdpi.com/2073-4344/9/9/713/s1>, Figure S1: XRD patterns of (a) SBA-15, (b) SBA-15-SH, (c) SBA-15-PY, and (d) SBA-15-Q; Figure S2: XRD patterns of (a) SBA-15, (b) SBA-15-Br, and (c) SBA-15-AEP; Figure S3: Nitrogen adsorption-desorption isotherms and the pore size distribution of (a) SBA-15, (b) SBA-15-SH, (c) SBA-15-PY, and (d) SBA-15-Q; Figure S4: Nitrogen adsorption-desorption isotherms and the pore size distribution of (a) SBA-15, (b) SBA-15-Br, and (c) SBA-15-AEP; Figure S5: TEM images of (a) SBA-15, (b) SBA-15-SH, (c) SBA-15-Br, (d) SBA-15-PY, (e) SBA-15-AEP, and (f) SBA-15-Q, perpendicular (left) and parallel (right) to the channels; Figure S6: <sup>13</sup>C CP/MAS NMR spectrum of SBA-15-Q and <sup>13</sup>C NMR spectrum of quinine; Figure S7: <sup>13</sup>C CP/MAS NMR spectrum of SBA-15-PY and <sup>13</sup>C NMR spectrum of (S)-(+)-prolinol; Figure S8: <sup>13</sup>C CP/MAS NMR spectrum of SBA-15-AEP and <sup>13</sup>C NMR spectrum of (S)-(-)-2-aminomethyl-1-ethylpyrrolidine; Figure S9 and description: <sup>29</sup>Si MAS NMR spectra of (a) SBA-15-SH and (b) SBA-15-Br; Figure S10: XRD pattern and TEM images of reused SBA-15-AEP in five runs; Figure S11: Nitrogen adsorption-desorption isotherms and the pore size distribution of reused SBA-15-AEP in five runs. Table S1: The specific surface area, pore volume, and pore diameter of mesoporous silica; Table S2: The density of chiral basic sites and the ratio of silanol to basic sites; Table S3: The molecular weight, molar fractions of Q<sup>i</sup> sites and the density of silanols for SBA-15-SH and SBA-15-Br, and product analysis.

**Author Contributions:** J.H. and Z.A. conceived and designed the experiments; L.C. performed the experiments; Y.J. contributed some of the data analysis and mechanism study; Z.A. wrote the paper.

**Funding:** Financial supports from the National Natural Science Foundation of China (21673016, 21521005), National Key R&D Program of China (2017YFB0307200), and the Fundamental Research Funds for the Central Universities are gratefully acknowledged.

**Conflicts of Interest:** The authors declare no conflict of interest.

## References

1. Witherup, K.M.; Ransom, R.W.; Graham, A.C.; Bernard, A.M.; Salvatore, M.J.; Lumma, W.C.; Anderson, P.S.; Pitzemberger, S.M.; Varga, S.L. Martinelline and Martinellic Acid, Novel g-Protein Linked Receptor Antagonists from the Tropical Plant *Martinella Iquitosensis*. *J. Am. Chem. Soc.* **1995**, *117*, 6682–6685. [[CrossRef](#)]

2. Sridharan, V.; Suryavanshi, P.A.; Menendez, J.C. Advances in the Chemistry of Tetrahydroquinolines. *Chem. Rev.* **2011**, *111*, 7157–7259. [[CrossRef](#)] [[PubMed](#)]
3. Weissman, A.; Muren, J.F. Depressant 1,2-dihydroquinolines and related derivatives. *J. Med. Chem.* **1971**, *14*, 49–53. [[CrossRef](#)] [[PubMed](#)]
4. Kothandaraman, P.; Foo, S.J.; Chan, P.W.H. Gold-Catalyzed Intramolecular Allylic Amination of 2-Tosylaminophenylprop-1-en-3-ols. A Concise Synthesis of (±)-Angustureine. *J. Org. Chem.* **2009**, *74*, 5947–5952. [[CrossRef](#)] [[PubMed](#)]
5. Yu, S.B.; Huang, Q.Q.; Luo, Y.; Lu, W. Total Synthesis of Camptothecin and SN-38. *J. Org. Chem.* **2012**, *77*, 713–717. [[CrossRef](#)] [[PubMed](#)]
6. Johnson, W.S.; Buell, B.G. 1,2-Dihydroquinoline. *J. Am. Chem. Soc.* **1952**, *74*, 4517–4520. [[CrossRef](#)]
7. Pearce, B.C.; Wright, J.J. Antihyperlipidemic/antioxidant dihydroquinolines. US Patent 5411969, 2 May 1995.
8. Campbell, R.H.; Wise, R.W.; Vaughn, W.A. Poly(6-oxy-2,2,4-trialkyl-1,2-dihydroquinoline) alkylene compounds as antidegradants for rubber. US Patent 4244864, 13 January 1981.
9. Zhao, P. Marketing Analysis for Ethoxiquin. *China Chem. Trade* **2013**, *1*, 277–278.
10. Liang, C.; Dai, M. Marketing Analysis for Ethoxiquin. *Anal. China Petrol. Chem. Ind. Eco.* **2014**, *41*, 143–145.
11. Kang, J.; Chen, X.L.; Wang, L.; Rampe, D. Ways to Fit a PK Model with Some Data Below the Quantification Limit. *J. Pharmacol. Exp. Ther.* **2001**, *28*, 481–504.
12. Kothandaraman, P.; Mothe, S.R.; Toh, S.S.M.; Chan, P.W.H. Gold-Catalyzed Cycloisomerizations of 1-(2-(Tosylamino)phenyl)prop-2-yn-1-ols to 1H-Indole-2-carbaldehydes and (E)-2-(Iodomethylene)indolin-3-ols. *J. Org. Chem.* **2011**, *76*, 7633–7640. [[CrossRef](#)]
13. Zhang, S.; Feng, J.; Kuo, S.; Brossi, A.; Hamel, E.; Tropsha, A.; Lee, K.H. Antitumor Agents. 199. Three-Dimensional Quantitative Structure-Activity Relationship Study of the Colchicine Binding Site Ligands Using Comparative Molecular Field Analysis. *J. Med. Chem.* **2000**, *43*, 167–176. [[CrossRef](#)] [[PubMed](#)]
14. Bhanja, C.; Jena, S.; Nayak, S.; Mohapatra, S. Organocatalytic tandem Michael addition reactions: A powerful access to the enantioselective synthesis of functionalized chromenes, thiochromenes and 1,2-dihydroquinolines. *Beilstein J. Org. Chem.* **2012**, *8*, 1668–1694. [[CrossRef](#)] [[PubMed](#)]
15. Luo, D.; Liu, J.; Zheng, L.; An, J.; Wang, W. Separation of Polycyclic Aromatic Hydrocarbons in Soft Pitch from Coal Tar and Its Compositions Analysis. *Coal. Chem. Ind.* **2011**, *39*, 1901–1905.
16. Long, R.; Schofield, K. Structure of a Silver-Bullvalene Complex1. *J. Am. Chem. Soc.* **1953**, *88*, 3161–3162. [[CrossRef](#)]
17. Wu, Y.; Liu, L.; Li, H.; Wang, D.; Chen, Y. Skraup-Doebner-Von Miller Duinoline Synthesis Revisited: Reversal of the Regiochemistry for Gamma-aryl-beta, gamma-Unsaturated alpha-Ketoesters. *J. Org. Chem.* **2006**, *71*, 6592–6595. [[CrossRef](#)]
18. Naoya, S.; Hidetoshi, T.; Yoshiji, T.; Kiyosei, T.; Shindoh, N.; Tokuyama, H.; Takemoto, Y. Triflic Imide Catalyzed (3+2) Cycloaddition of Aldimines with  $\alpha,\alpha$ -Dimethylallylsilane. *Cheminform* **2010**, *40*, 22–32.
19. Welsch, E.M.; Snyder, A.S.; Stockwell, B.R. Privileged Scaffolds for Library Design and Drug Discovery. *Curr. Opin. Chem. Biol.* **2010**, *14*, 347–361. [[CrossRef](#)]
20. Nammalwar, B.; Bunce, R.A. Recent Syntheses of 1,2,3,4-Tetrahydroquinolines, 2,3-Dihydro-4(1H)-quinolinones and 4(1H)-Quinolinones using Domino Reactions. *Molecules* **2013**, *19*, 204–232. [[CrossRef](#)]
21. Zhou, Y.G. Asymmetric Hydrogenation of Heteroaromatic Compounds. *Accounts Chem. Res.* **2007**, *40*, 1357–1366. [[CrossRef](#)]
22. Lei, A.; Waldkirch, J.P.; He, M.; Zhang, X. Highly Enantioselective Cycloisomerization of Enynes Catalyzed by Rhodium for the Preparation of Functionalized Lactams. *Angew. Chem. Int. Ed.* **2002**, *41*, 4526–4529. [[CrossRef](#)]
23. Yu, Z.; Jin, W.; Jiang, Q. Brønsted Acid Activation Strategy in Transition-Metal Catalyzed Asymmetric Hydrogenation of N-Unprotected Imines, Enamines, and N-Heteroaromatic Compounds. *Angew. Chem. Int. Ed.* **2012**, *51*, 6060–6072. [[CrossRef](#)]
24. Murata, S.; Sugimoto, T.; Matsuura, S. Hydrogenation and Hydrosilylation of Quinoxaline by Homogeneous Rhodium Catalysts. *Heterocycles* **1987**, *26*, 763. [[CrossRef](#)]
25. Hatano, M.; Mikami, K. Highly Enantioselective Quinoline Synthesis via Ene-type Cyclization of 1,7-Enynes Catalyzed by a Cationic BINAP–Palladium(II) Complex. *J. Am. Chem. Soc.* **2003**, *125*, 4704–4705. [[CrossRef](#)]

26. Li, Z.W.; Wang, T.L.; He, Y.M.; Wang, Z.J.; Fan, Q.H.; Pan, J.; Xu, L.J. Air-Stable and Phosphine-Free Iridium Catalysts for Highly Enantioselective Hydrogenation of Quinoline Derivatives. *Org. Lett.* **2008**, *10*, 5265–5268. [[CrossRef](#)]
27. Jensen, K.L.; Dickmeiss, G.; Donslund, B.S.; Poulsen, P.H.; Jørgensen, K.A. Asymmetric Organocatalytic Synthesis of Complex Cyclopenta[b]quinoline Derivatives. *Org. Lett.* **2011**, *13*, 3678–3681. [[CrossRef](#)]
28. Yoshiji, T. Development of Chiral Thiourea Catalysts and Its Application to Asymmetric Catalytic Reactions. *Chem. Pharm. Bull.* **2010**, *58*, 593–598.
29. Sundén, H.; Rios, R.; Ibrahim, I.; Eriksson, L.; Córdova, A.; Zhao, G.L.; Zhao, G. A Highly Enantioselective Catalytic Domino Aza-Michael/Aldol Reaction: One-Pot Organocatalytic Asymmetric Synthesis of 1,2-Dihydroquinolidines. *Chemistry* **2007**, *38*, 827–832.
30. Li, H.; Wang, J.; Xie, H.; Zu, L.; Jiang, W.; Duesler, E.N.; Wang, W. Chiral Diphenylprolinol TES Ether Promoted Conjugate Addition–Aldol-Dehydration Reactions between  $\alpha,\beta$ -Unsaturated Aldehydes and 2-N-Protected Amino Benzaldehydes. *Org. Lett.* **2007**, *9*, 965–968. [[CrossRef](#)]
31. Yoshitomi, Y.; Arai, H.; Makino, K.; Hamada, Y. Enantioselective synthesis of martinelline chiral core and its diastereomer using asymmetric tandem Michael–aldol reaction. *Tetrahedron* **2008**, *64*, 11568–11579. [[CrossRef](#)]
32. Zhang, W.; Wang, Y.F.; Luo, S.P.; Li, B.L.; Xia, A.B.; Zhong, A.G.; Xu, D.Q.; Wang, Y.; Luo, S.; Li, B.; et al. One-Pot Organocatalytic Asymmetric Synthesis of 3-Nitro-1,2-dihydroquinolines by a Dual-Activation Protocol. *Chem. Asian J.* **2009**, *4*, 1834–1838.
33. Liu, X.; Lu, Y. Bi-functional Thiourea-Promoted Cascade aza-Michael-Henry-Dehydration Reactions: Asymmetric Preparation of 3-Nitro-1,2-Dihydroquinolines. *Org. Biomol. Chem.* **2010**, *8*, 4063–4069. [[CrossRef](#)]
34. Notestein, J.M.; Katz, A. Enhancing Heterogeneous Catalysis through Cooperative Hybrid Organic–Inorganic Interfaces. *Chem. A Eur. J.* **2006**, *12*, 3954–3965. [[CrossRef](#)]
35. Margelefsky, E.L.; Zeidan, R.K.; Davis, M.E. Cooperative catalysis by silica-supported organic functional groups. *Chem. Soc. Rev.* **2008**, *37*, 1118. [[CrossRef](#)]
36. Estrada, M.R.B.; Escudero, A. Amino Groups Immobilized on Silica Gel: An Efficient and Reusable Heterogeneous Catalyst for the Knoevenagel Condensation. *J. Chem. Soc. Perkin. Trans.* **1989**, *47*, 105–107.
37. Ken, M.; Mizuki, T.; Yasuhiro, I. Heterogeneous Organic Base-Catalyzed Reactions Enhanced by Acid Supports. *J. Am. Chem. Soc.* **2007**, *129*, 9540–9541.
38. Bass, J.D.; Andrew, S.; Pascall, A.J.; Alexander, K. Acid-Base Bi-functional and Dielectric Outer-Sphere Effects in Heterogeneous Catalysis: A Comparative Investigation of Model Primary Amine Catalysts. *J. Am. Chem. Soc.* **2006**, *128*, 3737–3747. [[CrossRef](#)]
39. Johan, A.; Ahmad, M.; Catherine, R.; Corriu, R.J.P. Mesoporous Materials with an Acidic Framework and Basic Pores. A Successful Cohabitation. *J. Am. Chem. Soc.* **2006**, *128*, 8718–8719.
40. Jin, R.; Zheng, D.; Liu, R.; Liu, G. Silica-Supported Molecular Catalysts for Tandem Reactions. *Chem. Cat. Chem.* **2018**, *10*, 1739–1752. [[CrossRef](#)]
41. Cao, H.; Zhu, X.; Wang, D.; Sun, Z.; Deng, Y.; Hou, X.; Zhao, D. Selectivity Enhancement in Dynamic Kinetic Resolution of Secondary Alcohols through Adjusting the Micro-Environment of Metal Complex Confined in Nanochannels: A Promising Strategy for Tandem Reactions. *ACS Catal.* **2015**, *5*, 27–33. [[CrossRef](#)]
42. An, Z.; He, J.; Dai, Y.; Yu, C.; Li, B.; He, J. Enhanced Heterogeneous Asymmetric Catalysis via the Acid–Base Cooperation between Achiral Silanols of Mesoporous Supports and Immobilized Chiral Amines. *J. Catal.* **2014**, *317*, 105–113. [[CrossRef](#)]
43. Yang, S.; He, J. Heterogeneous Asymmetric Henry–Michael One-Pot Reaction Synergistically Catalyzed by Grafted Chiral Bases and Inherent Achiral Hydroxyls on Mesoporous Silica Surface. *Chem. Commun.* **2012**, *48*, 10349–10351. [[CrossRef](#)]
44. Wang, S.S.; He, J.; An, Z. Heterogeneous Enantioselective Synthesis of Chromans via the oxa-Michael–Michael Cascade Reaction Synergistically Catalyzed by Grafted Chiral Bases and Inherent Hydroxyls on Mesoporous Silica Surface. *Chem. Commun.* **2017**, *53*, 8882–8885. [[CrossRef](#)]
45. An, Z.; Dai, Y.; Jiang, Y.; He, J. Asymmetric Knoevenagel–Phospha-Michael Tandem Reaction Synergistically Catalyzed by Achiral Silanols and Grafted Chiral Amines on Mesoporous Silica. *Asian J. Org. Chem.* **2019**. [[CrossRef](#)]
46. Zhao, D.; Melosh, N.; Feng, J.; Huo, Q.; Fredrickson, G.H.; Chmelka, B.F.; Stucky, G.D. Triblock Copolymer Syntheses of Mesoporous Silica with Periodic 50 to 300 Angstrom Pores. *Science* **1998**, *279*, 548–552. [[CrossRef](#)]

47. Xu, D.Q.; Wang, Y.F.; Luo, S.P.; Zhang, S.; Zhong, A.G.; Chen, H.; Xu, Z.Y. A Novel Enantioselective Catalytic Tandem Oxa-Michael-Henry Reaction: One-Pot Organocatalytic Asymmetric Synthesis of 3-Nitro-2H-chromenes. *Adv. Synth. Catal.* **2008**, *350*, 2610–2616. [[CrossRef](#)]
48. Jones, M.D.; Raja, R.; Thomas, J.M.; Johnson, B.F.G.; Lewis, D.W.; Rouzaud, J.; Harris, K.D.M. Enhancing the Enantioselectivity of Novel Homogeneous Organometallic Hydrogenation Catalysts. *Angew. Chem.* **2003**, *115*, 4462–4467. [[CrossRef](#)]
49. Yin, G.; Zhang, R.; Li, L.; Tian, J.; Chen, L. One-Pot Enantioselective Synthesis of 3-Nitro-2H-chromenes Catalyzed by a Simple 4-Hydroxyprolinamide with 4-Nitrophenol as Cocatalyst. *Eur. J. Org. Chem.* **2013**, *24*, 5431–5438. [[CrossRef](#)]
50. Yua, X.; Wang, W. Organocatalysis: Asymmetric Cascade Reactions Catalysed by Chiral Secondary Amines. *Org. Biomol. Chem.* **2008**, *6*, 2037–2046. [[CrossRef](#)]
51. Bahmanyar, S.; Houk, K.N. The Origin of Stereoselectivity in Proline-Catalyzed Intramolecular Aldol Reactions. *J. Am. Chem. Soc.* **2001**, *123*, 12911–12912. [[CrossRef](#)]
52. Crudden, C.M.; Sateesh, M.; Lewis, R. Mercaptopropyl-Modified Mesoporous Silica: A Remarkable Support for the Preparation of a Reusable, Heterogeneous Palladium Catalyst for Coupling Reactions. *J. Am. Chem. Soc.* **2005**, *127*, 10045–10050. [[CrossRef](#)]
53. Yu, P.; He, J.; Yang, L.; Pu, M.; Guo, X. Stepwise Fabrication and Architecture of Heterogeneous 9-Thiourea Epiquinine Catalyst with Excellent Enantioselectivity in the Asymmetric Friedel-Crafts Reaction of Indoles with Imines. *J. Catal.* **2008**, *260*, 81–85. [[CrossRef](#)]
54. Yu, P.; He, J.; Yang, L.; Pu, M.; Guo, X. 9-Thiourea Cinchona Alkaloid Supported on Mesoporous Silica as a Highly Enantioselective, Recyclable Heterogeneous Asymmetric Catalyst. *Chem. Commun.* **2008**, *20*, 2355–2357. [[CrossRef](#)]
55. Tommaso, M.; Richard, N.; Haas, V.; Henk, H. Asymmetric Organocatalytic Henry Reaction. *Angew. Chem. Int. Ed.* **2006**, *45*, 929–931.



© 2019 by the authors. Licensee MDPI, Basel, Switzerland. This article is an open access article distributed under the terms and conditions of the Creative Commons Attribution (CC BY) license (<http://creativecommons.org/licenses/by/4.0/>).